平成30年度極域・中緯度SuperDARN研究集会(2018年10月16-17日、宇宙地球環境研究所)

磁気圏電場の中低緯度電離圏への侵入
Penetration of the magnetospheric electric fields to the middle and low latitude ionosphere

菊池 崇

Takashi Kikuchi

Electric fields are observed with the Hokkaido SuperDARN and HF Doppler sounders at middle and low latitudes and with magnetometers at the equator

$$\Delta f = -\frac{2f}{c}\frac{E}{B}\sin\theta\cos I$$

$f = 5$ [MHz], $I = 49°$, $B = 46000$ [nT]

$\theta = 78.2°$ (distance = 120, reflection height = 300km)

$V_{vert} = -30.6\ \Delta f$ [m/s]

$E = -2.15\ \Delta f$ [mV/m]

HF Doppler (HFD) sounder in Tokyo

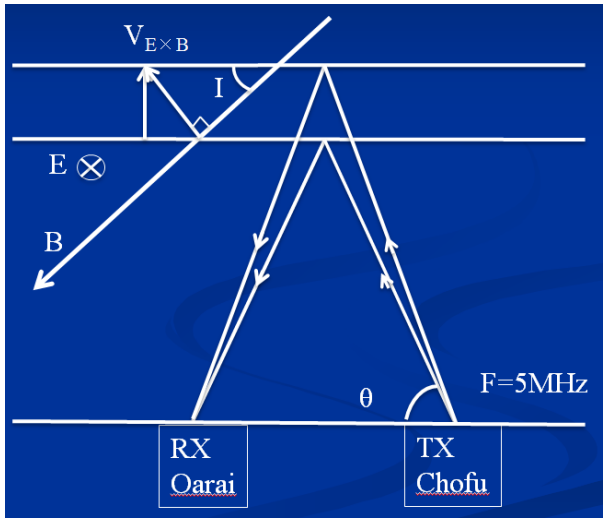

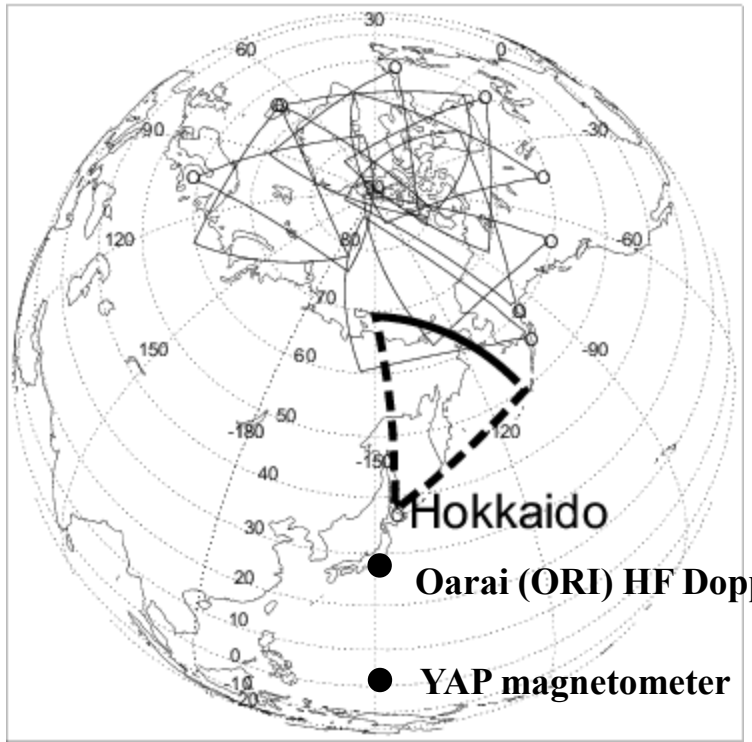

We would see good correlation between the middle-low latitude electric fields and the equatorial electrojet (EEJ), if the electric fields are transmitted from the polar ionosphere.

$$EEJ = \sigma_C \cdot E_{penetrated}$$

Cowling conductivity: $\sigma_C = \sigma_P + \frac{\sigma_H^2}{\sigma_P}$

Dynamos of the Region-1 and -2 field-aligned currents

(a) Global MHD simulation of the dynamos of the R1 and R2 FACs filled with high pressure plasma (red and white regions) around the cusp/mantle and near-Earth plasma sheet, respectively. (The red and black lines indicate dynamo currents and FACs with negative and positive J · E, respectively)

(b) Distribution of the R1 and R2 FACs in the northern polar ionosphere. Solid and dotted contours represent inward and outward currents, respectively.

(c) Electric potential distribution in the polar ionosphere. Dashed and solid contours represent positive and negative potentials, respectively.

Tanaka (1995)

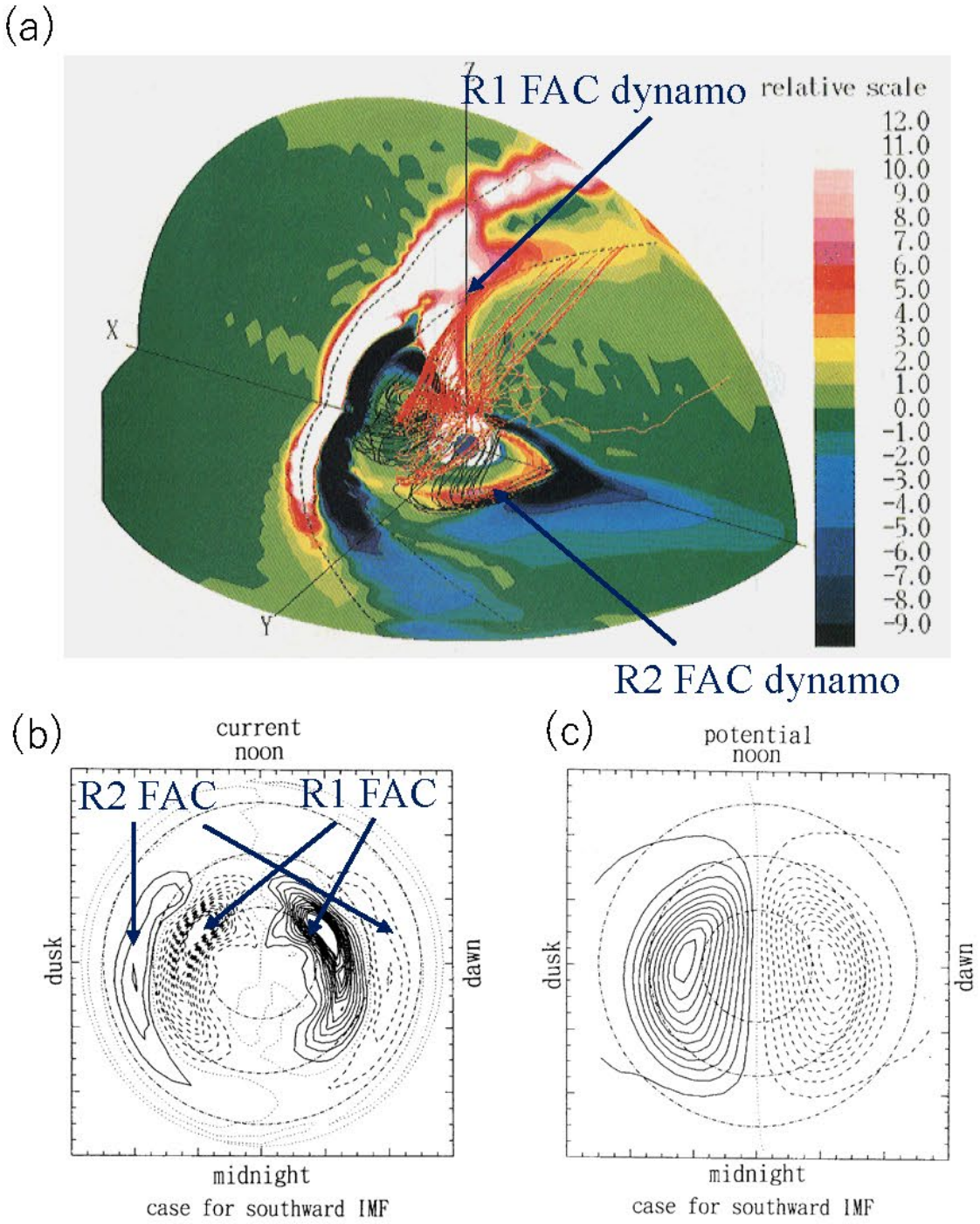

Penetration of DP2 and substorm electric fields to mid and equatorial latitudes as observed by magnetometers

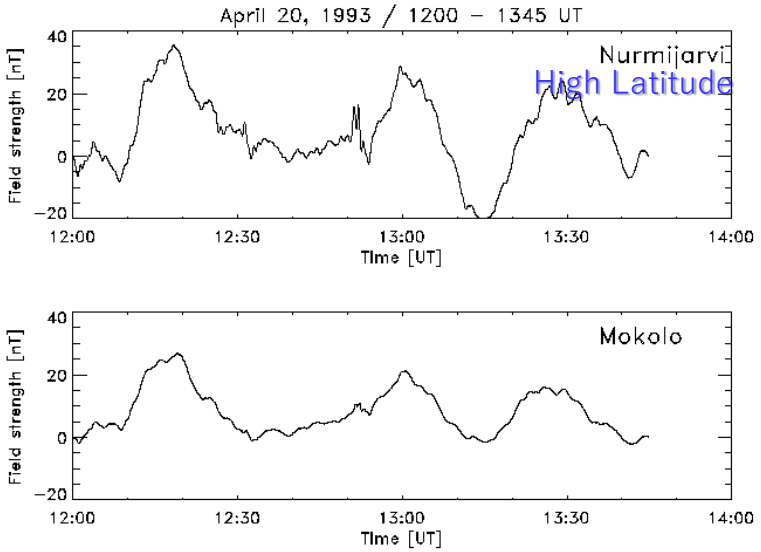

R = 0.9

T = 25 sec

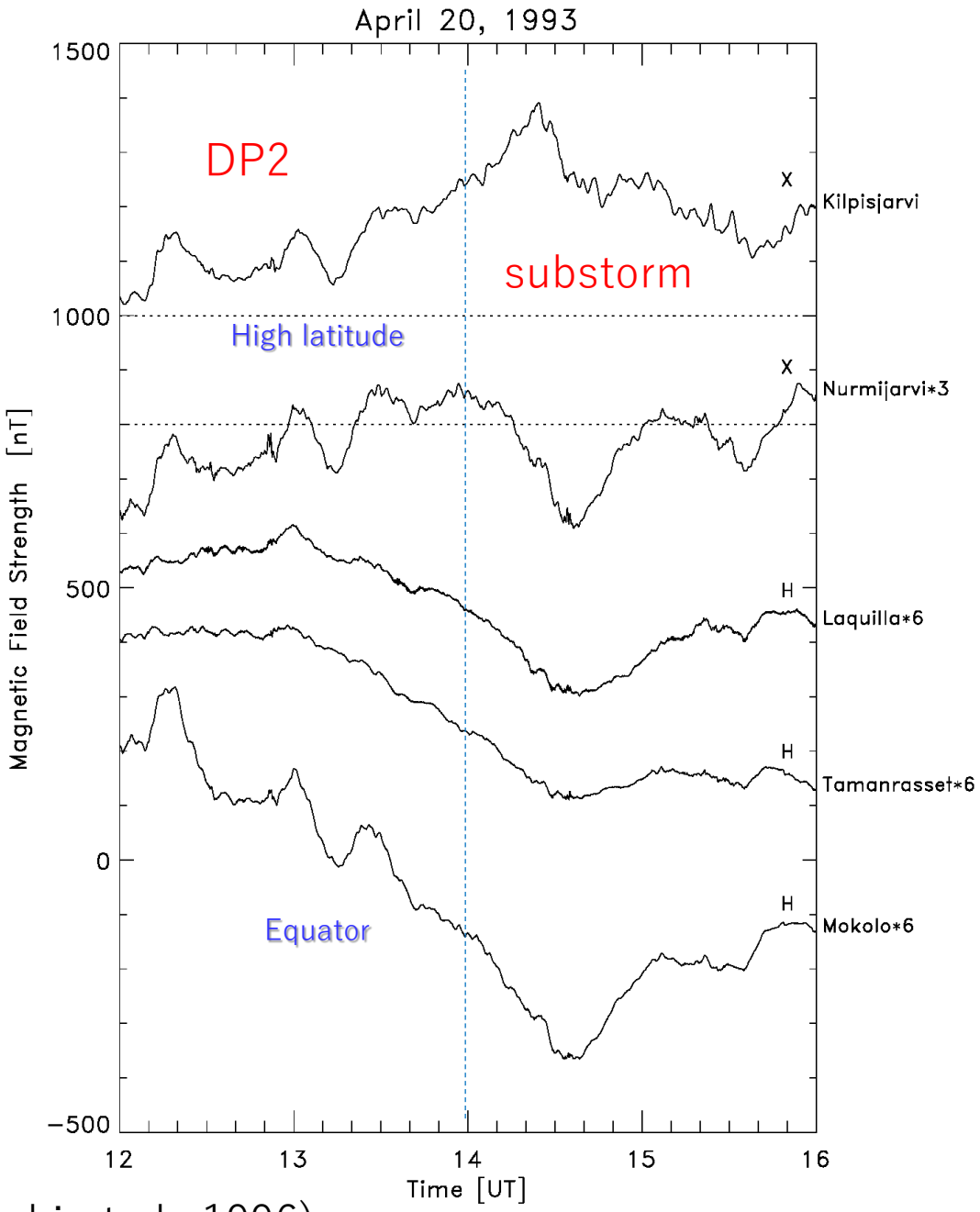

Quasi-periodic fluctuations during the interval 1200-1345 UT appear coherently at auroral and equatorial latitudes, while no significant fluctuations are observed at mid and low latitudes.

(Kikuchi et al., 1996)

DP2 fluctuations attenuate geometrically during propagation to low latitude with amplification at the equator

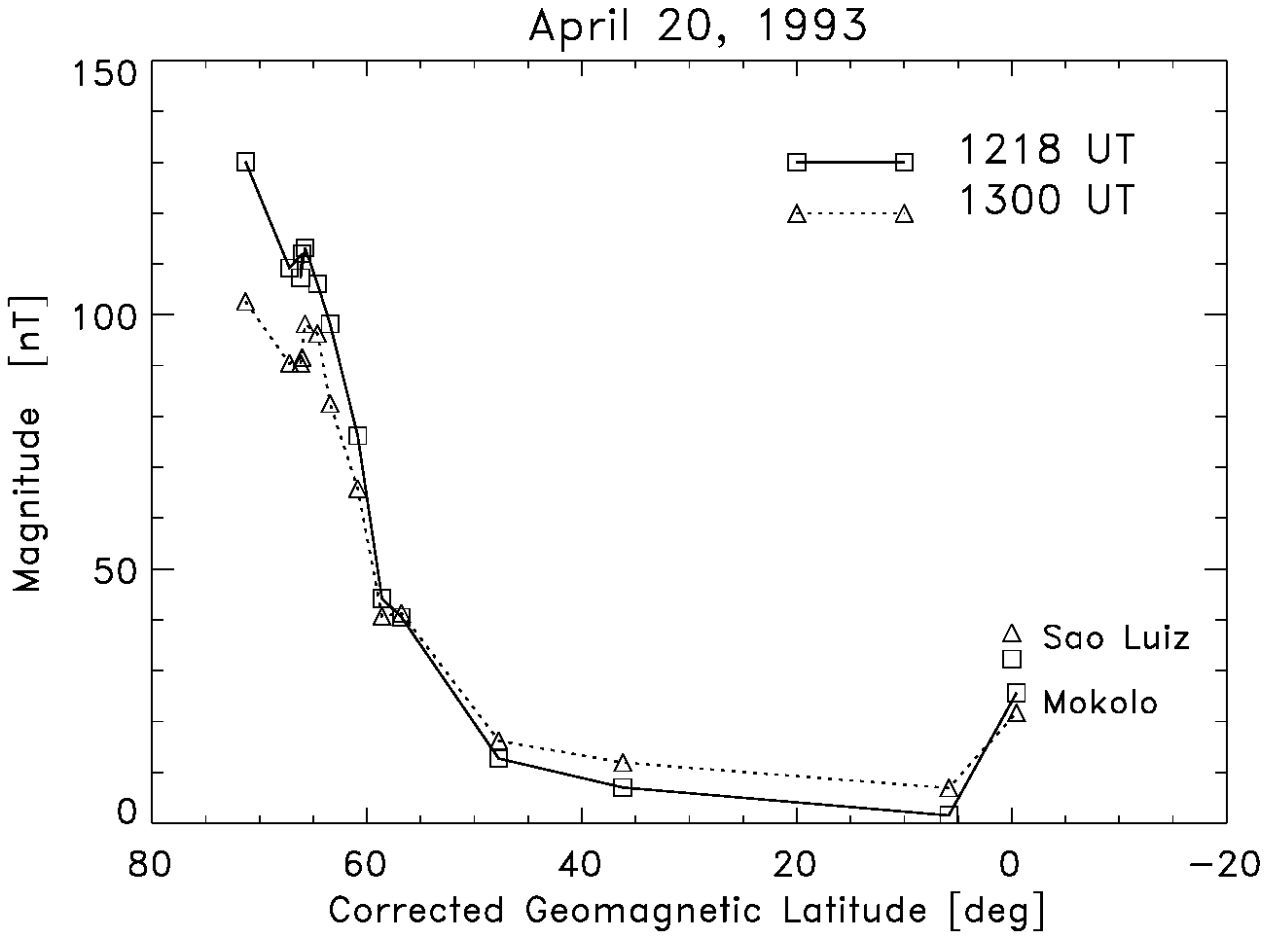

Latitudinal profile of the magnitude of the DP2 fluctuations shown in Figure 2. The DP2 decreases with decreasing latitude because of the geometrical attenuation, while significantly enhanced by the Cowling effect at the equator with magnitude comparable to those at subauroral latitude. (Kikuchi et al., 1996)

Region-1 field-aligned current-equatorial electojet circuit

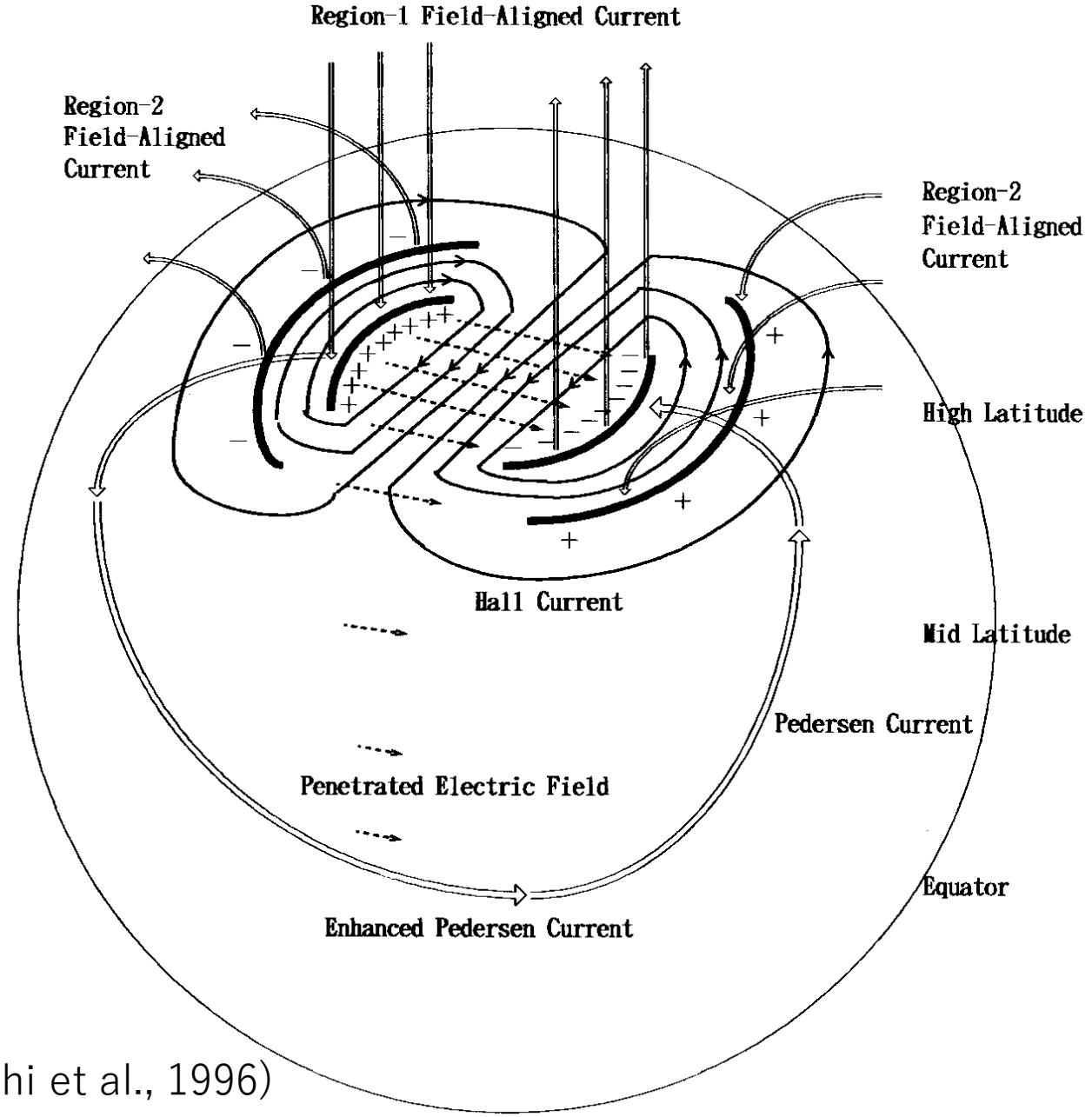

A schematic diagram of the DP2 ionospheric currents under the southward IMF condition, composed of the two-cell Hall currents at high latitudes surrounding the R1 FACs and the Pedersen current circuit from the R1 FACs to the equatorial ionospheric currents enhanced by the Cowling effect (EEJ).

(Kikuchi et al., 1996)

DP2 and substorm electric fields (EISCAT observation)

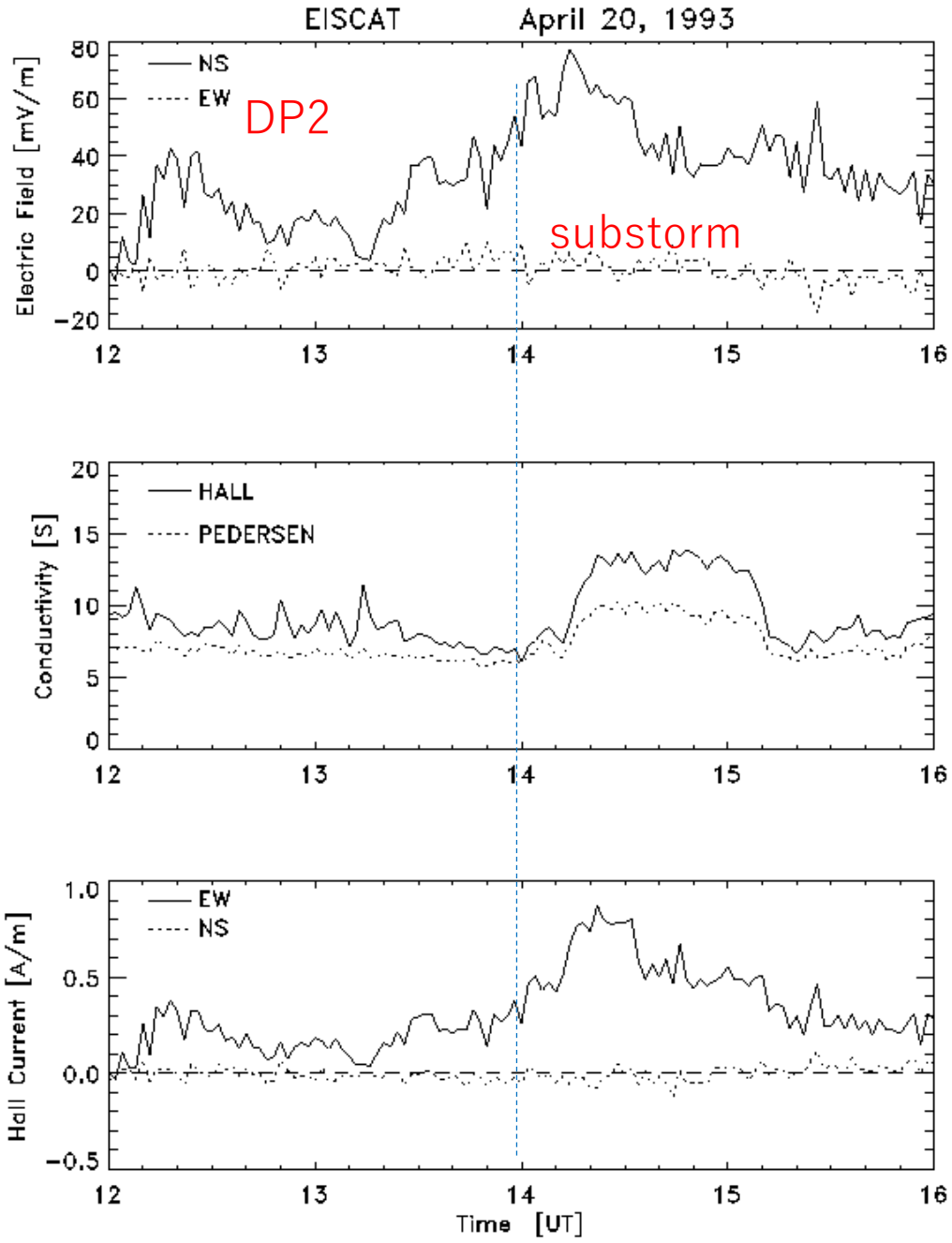

The NS and EW components of the electric field (upper panel), the Hall and Pedersen conductivities (middle panel) observed by the EISCAT radar in Scandinavia, and the NS and EW components of the Hall current calculated from the observed electric field and Hall conductivity (lower panel) for the time interval of 12 - 16 UT. Fluctuations corresponding to the DP2 variation are recognized in the NS component of the electric field, while the conductivity remains at the undisturbed level.

(Kikuchi et al., 1996)

Electric fields of the R1 and R2 FACs deduced form EISCAT and IMAGE observations

Convection (E_1) and Shielding (E_2) electric fields

Convection (E_1) and shielding (E_2) electric fields depicted with the solid and dotted lines, respectively, at the auroral (EISCAT) and subauroral (Nurmijarvi) latitudes as deduced from the electric field measured by EISCAT and IMAGE magnetometer array data for the substorm event in Figure 2 (14-16 UT). E_1 dominates over E_2 at both latitudes prior to the substorm (12-14 UT), while E_2 is intensified during the substorm and dominates over the geometrically attenuated convection electric field (E_1*0.40) at Kilpisjarvi.

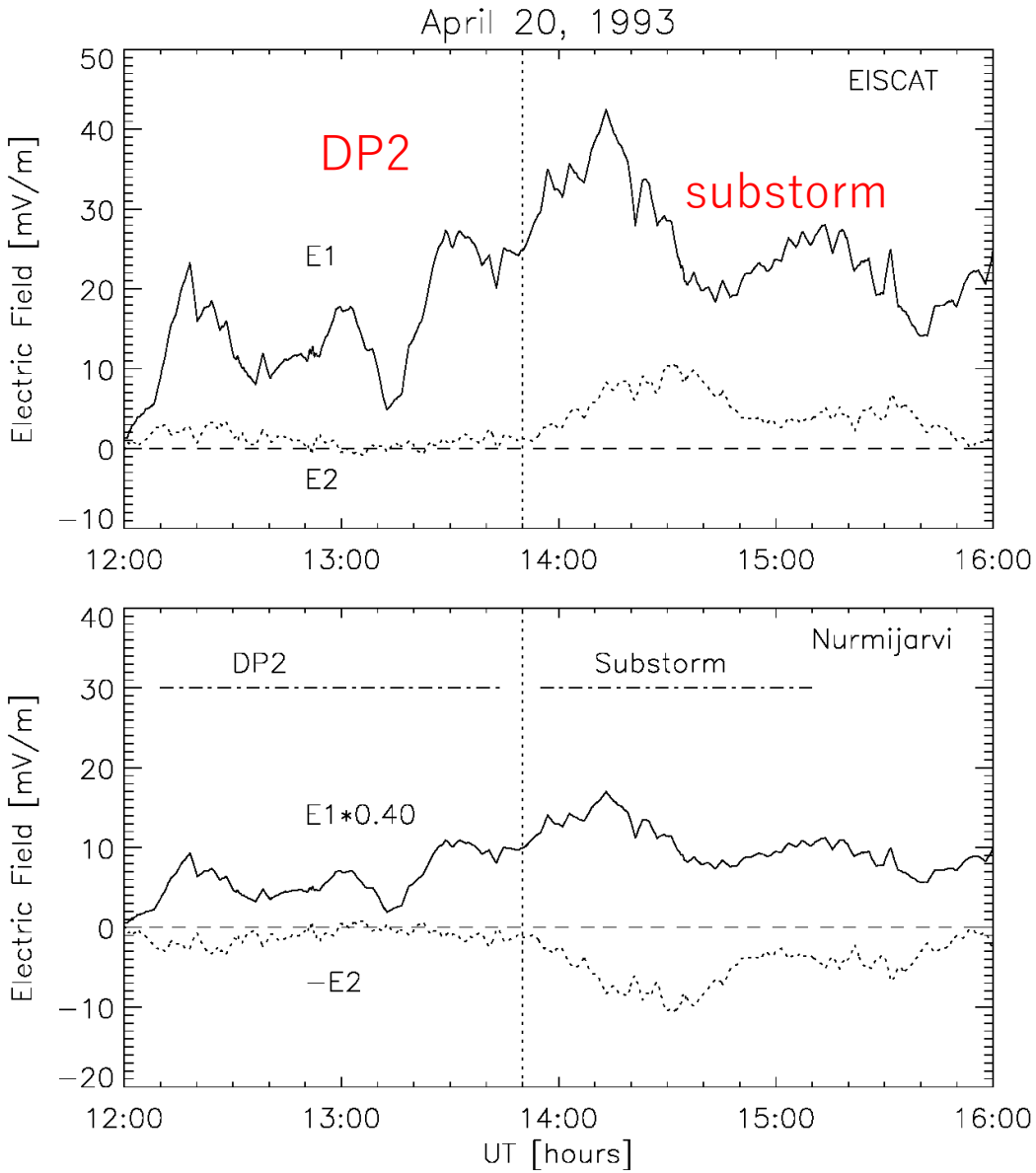

(Kikuchi et al., 2000)

Current circuit between the partial ring current and equatorial CEJ established during the substorm

Schematic diagram of the substorm overshielding current circuit composed of the partial ring current, R2 FACs and equatorial CEJ. High latitude overshielding currents are the Hall currents surrounding the R2 FACs in the same way as the DP2 currents surround the R1 FACs. (Figure 11 of

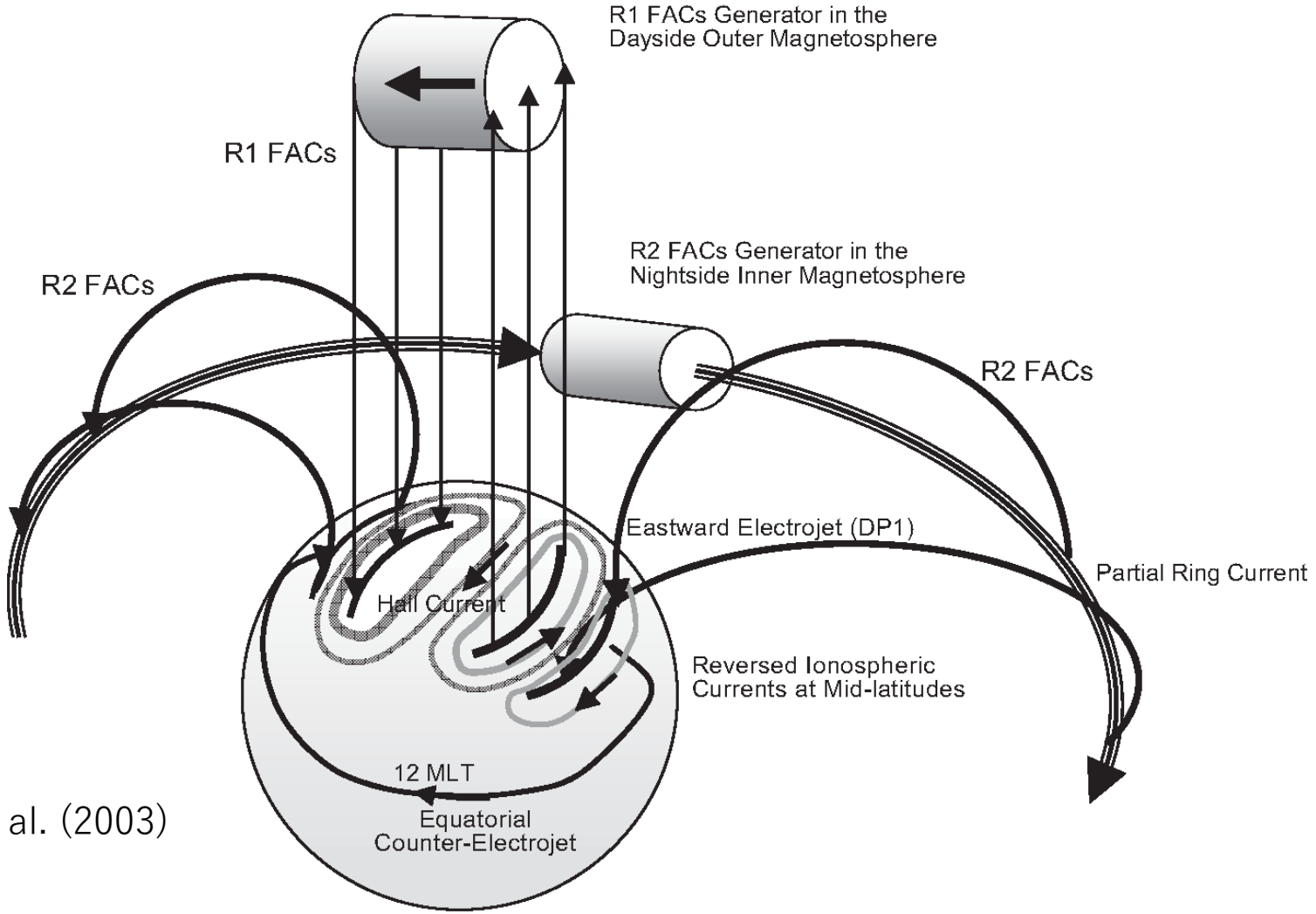

Kikuchi et al. (2003)

Equatorial DP2 fluctuations caused by the EEJ (R1 FACs) and CEJ (R2 FACs) electric fields

(top) Solar wind dynamic pressure, (middle) IMF Bz measured by ACE 32 min prior to the DP 2 fluctuation event, and (bottom) the equatorial electrojet defined as H (YAP) – H (OKI). The DP 2 fluctuations are composed of EEJ and CEJ, corresponding to the southward and northward IMF, respectively.

Kikuchi et al. (2010)

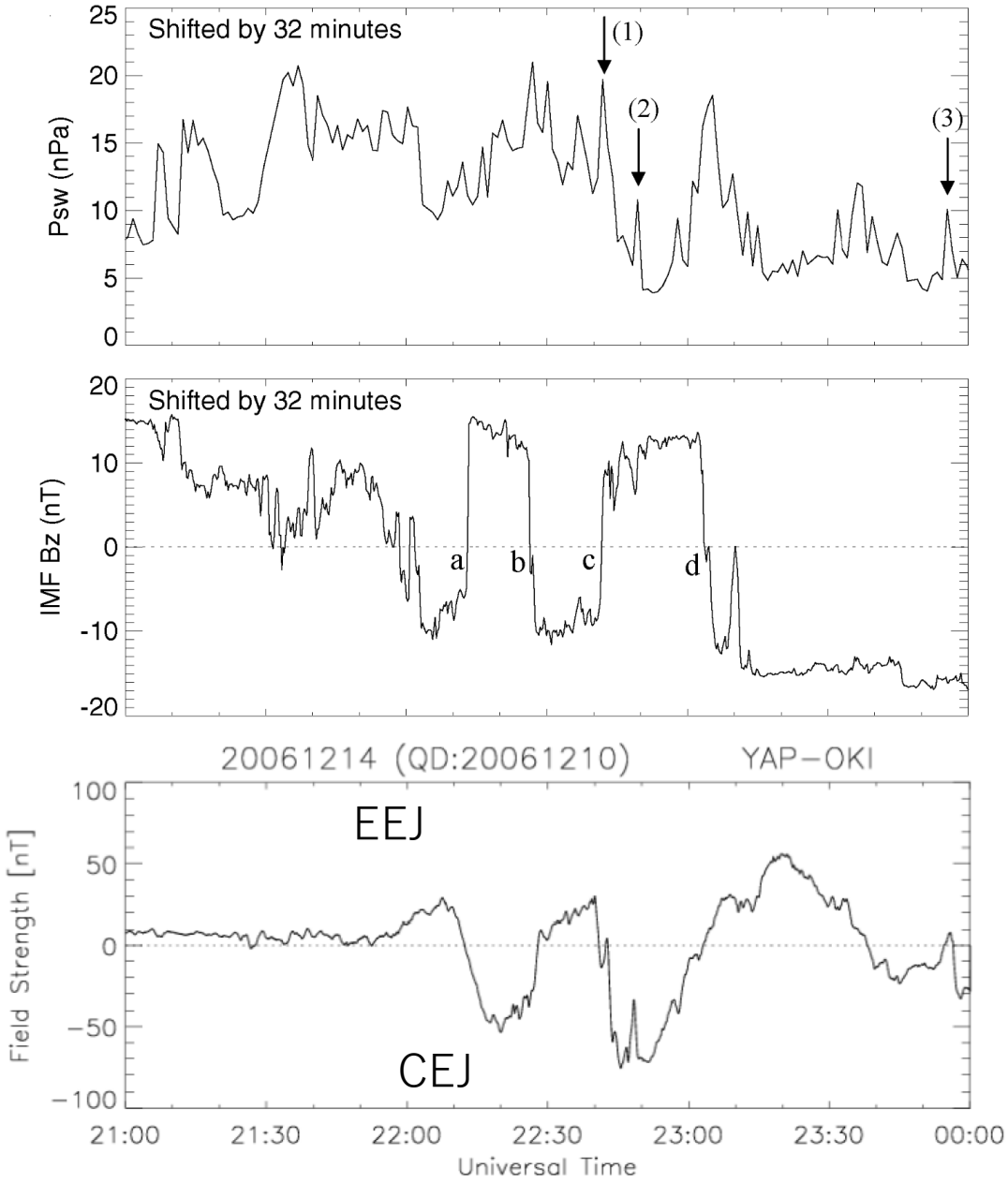

Hokkaido radar observation of the convection and overshielding electric field corresponding to EEJ and CEJ, respectively

UT versus latitude plots of the line - of - sight velocity measured by beam 9 of the Hokkaido radar during the DP2 fluctuations shown in Figure 5. Cool and warm colors indicate plasma motion toward and away from the radar, caused by the westward and eastward electric fields, respectively.

Kikuchi et al. (2010)

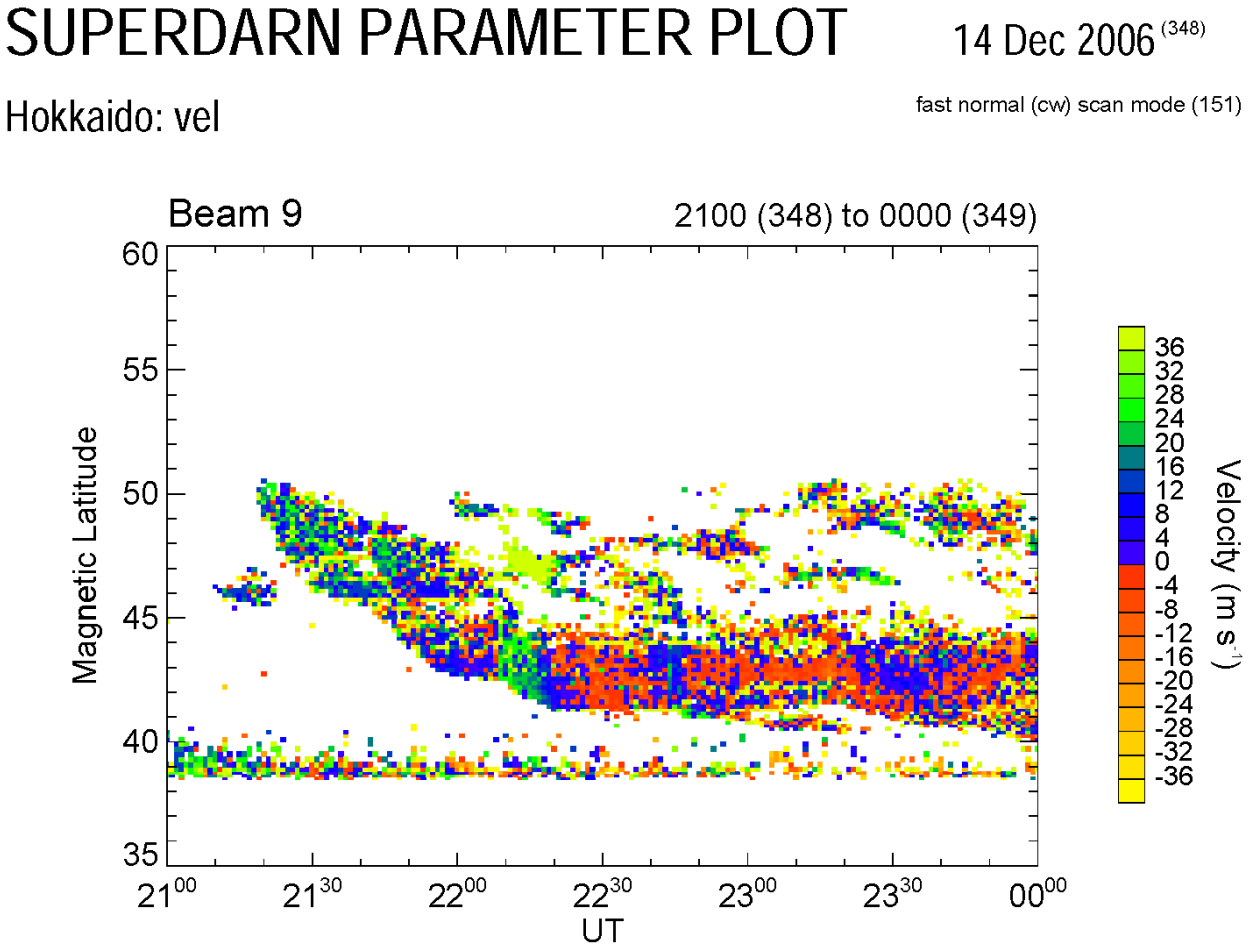

2-cell and 4-cell convection vortices corresponding to EEJ and CEJ of the DP2 event -SuperDARN observation -

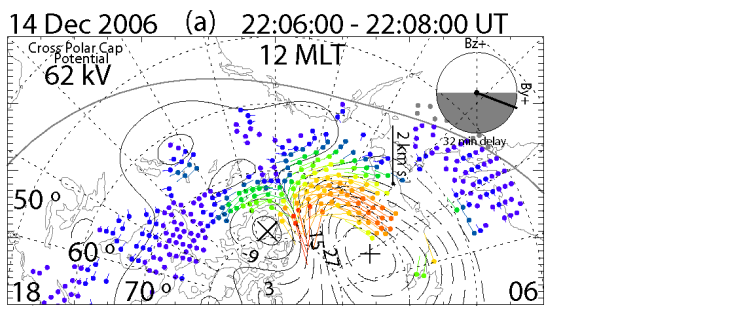

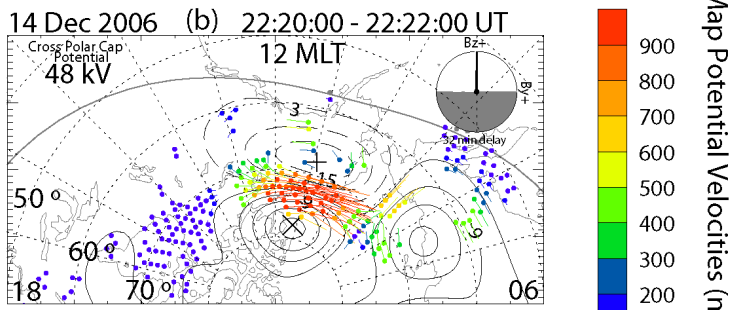

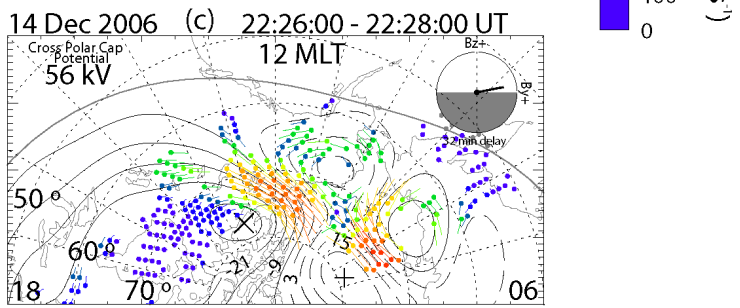

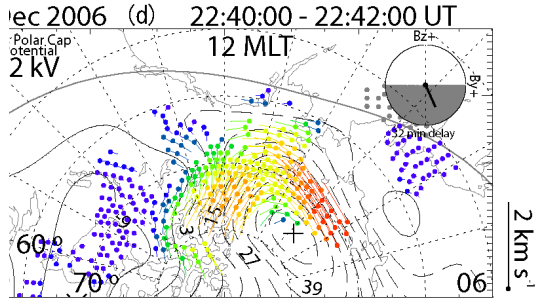

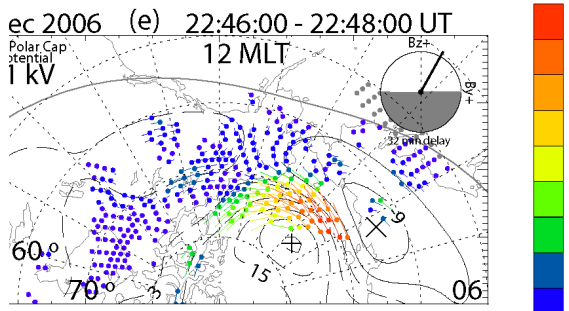

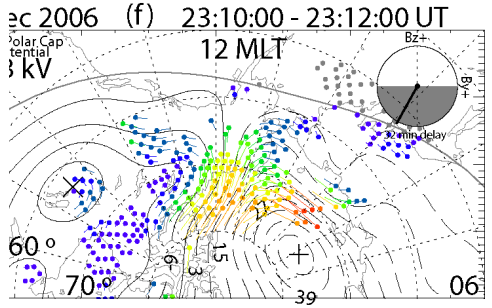

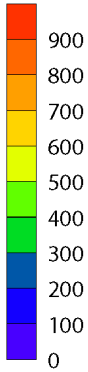

Kikuchi et al. (2010)

Substorm overshielding (R2 FACs) electric fields at low latitude observed by the HF Doppler sounder

(a) H component of the magnetic field at low latitude, Okinawa, Japan (OKI; dotted curve), dip equator, Yap, Micronesia (YAP; solid curve) in the western Pacific zone on the nightside and (b) at the dip equator, Sao Luiz, Brazil (SLZ), 12 h behind YAP on the dayside. The substorm positive bay started at 1600 UT at OKI and YAP, when the westward CEJ developed at SLZ. (c) The electric field measured by the HF Doppler sounder at Sugadaira, Japan (SGD), on the nightside (0030–0300 MLT), which is low-pass filtered with the window of 80 s. Eastward overshielding electric field starts to increase at 1600 UT and again at 1635 UT, simultaneously with the dayside CEJs.

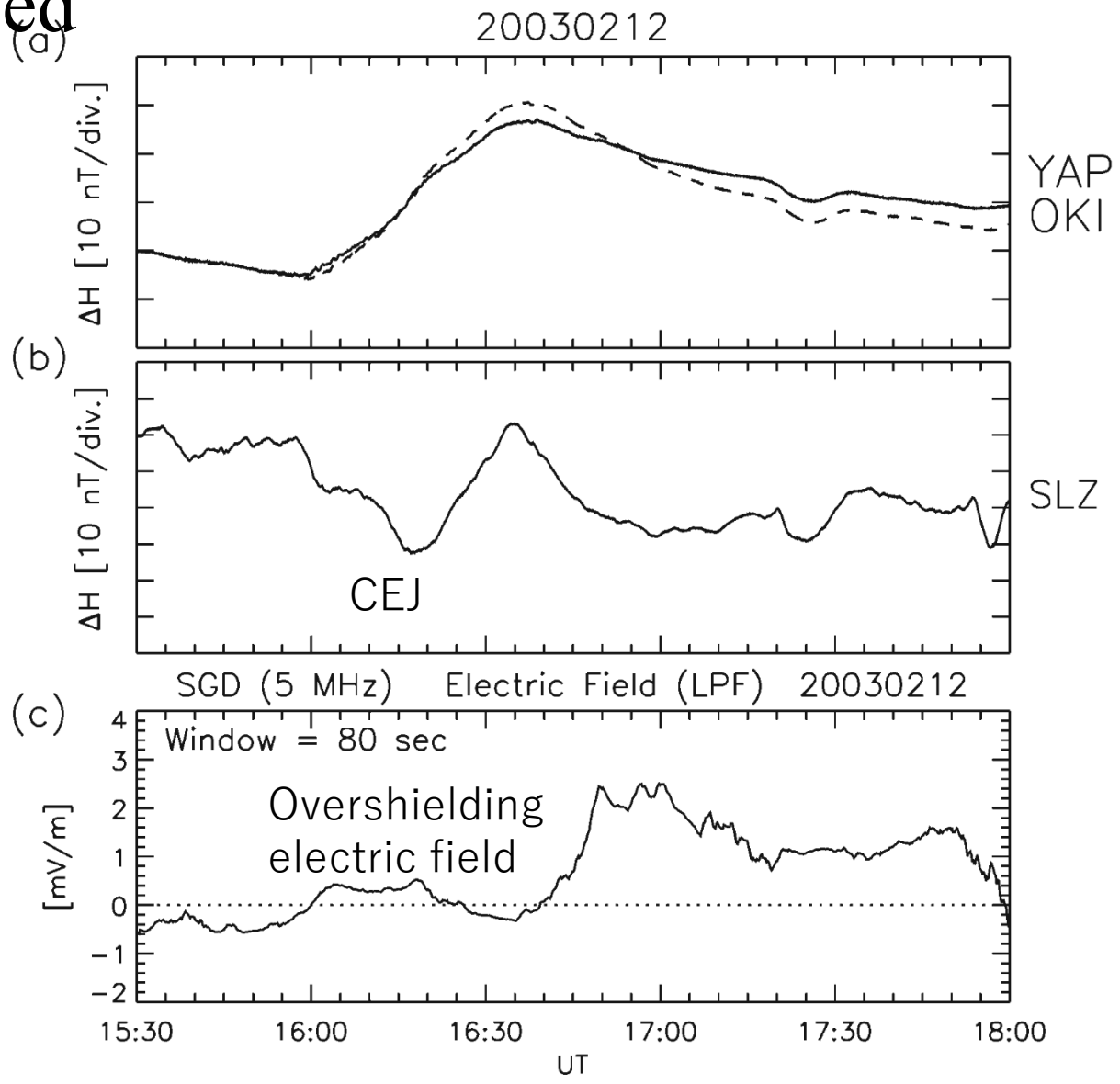

Hashimoto et al. (2017)

Equatorial enhancement of the geomagnetic storm caused by equatorial ionospheric currents

Geomagnetic storm recorded at low latitude, Okinawa (OKI) and equator, Guam (GAM) and Yap, Micronesia (YAP) in the western Pacific region. The storm is enhanced at YAP with an enhancement ratio of 2.7, caused by combined effects of the main phase EEJ and recovery phase CEJ.

Kikuchi et al. (2008)

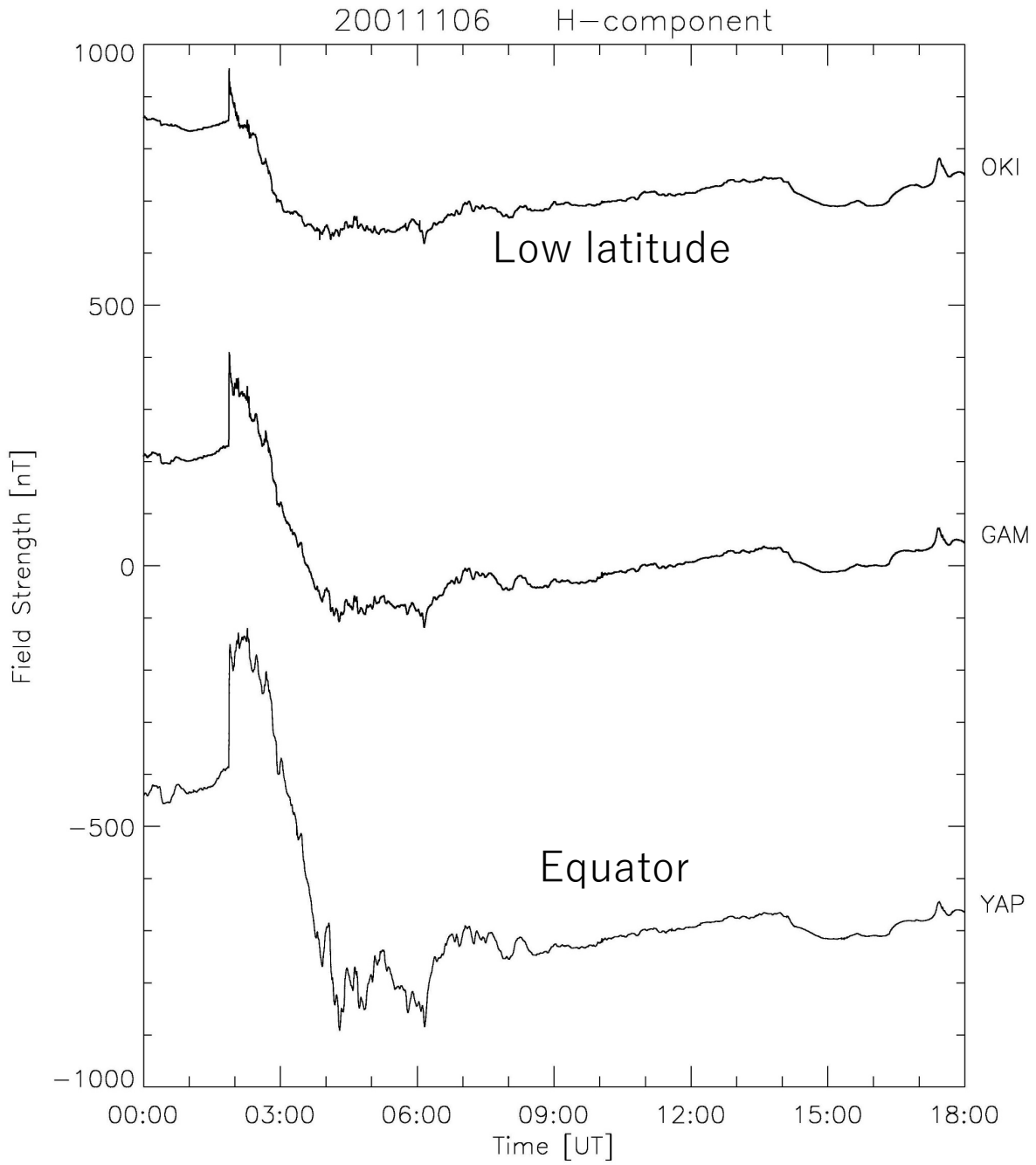

Main phase EEJ and recovery phase CEJ

(top) Contour map of the magnetic disturbances caused by the westward auroral electrojet (AEJ) in the dawn sector derived from the IMAGE magnetometer array data and (bottom) the equatorial electrojets obtained from H(YAP) by subtracting H(OKI) after eliminating quiettime diurnal variations. The AEJs developed at middle latitude (55° corrected geomagnetic latitude (CGM)) during the main phase, while they shift to the auroral latitude (65° CGM) during the recovery phase. The equatorial electrojets are composed of the EEJ and CEJ during the main and recovery phases, respectively. (Figure 8 of Kikuchi et al. (2008))

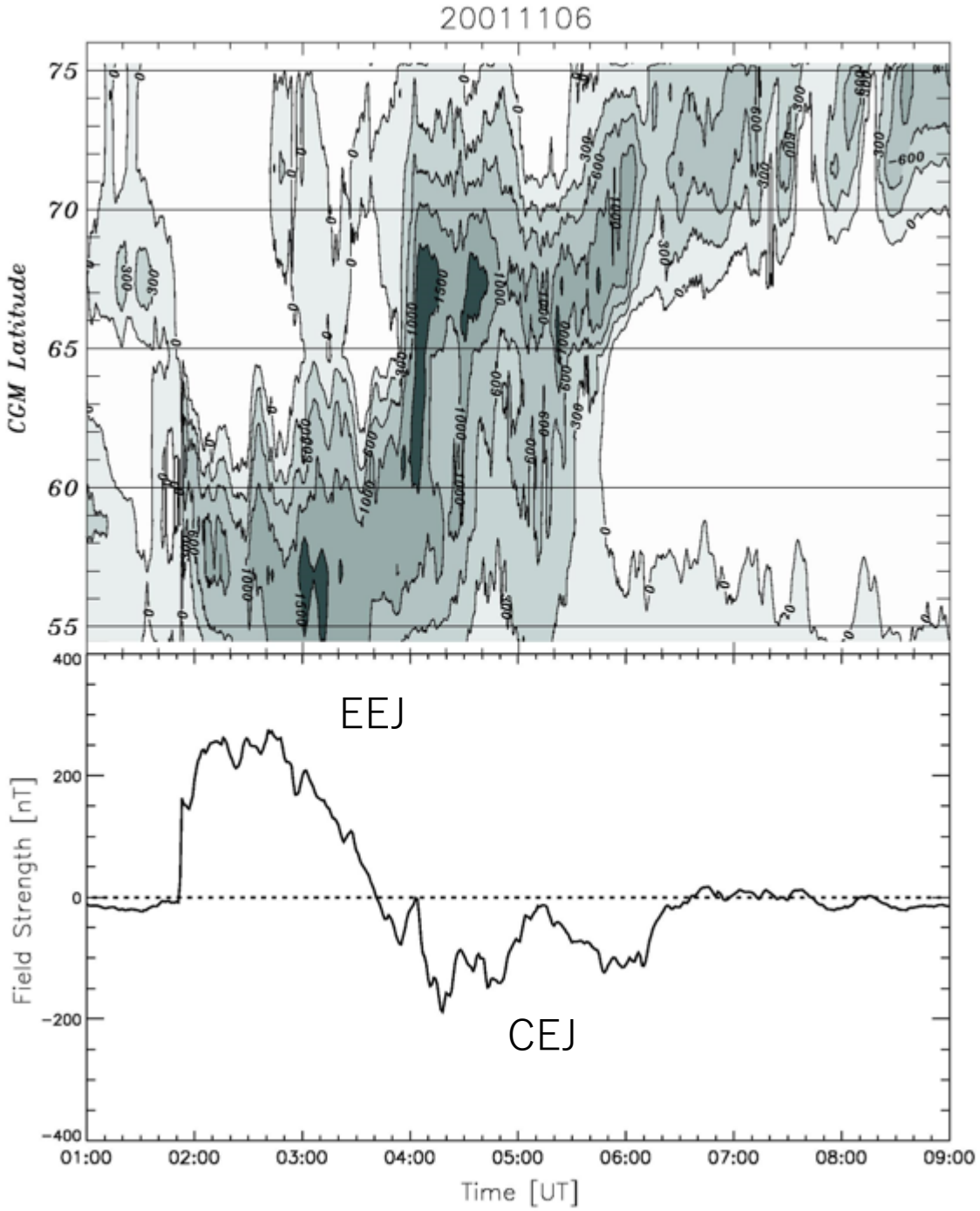

Stormtime electric fields at the equator observed by Jicamarca IS radar

(from the top) Solar wind dynamic pressure, IMF Bz, IEF, ASY/SYM-H, equatorial electrojet (YAP-OKI) in the western Pacific and Jicamarca vertical plasma drifts during 9–10 November 2004. The dashed curves denote the quiet time patterns, and the large circles indicate local noon. The electric field is over 3 mV/m during the storm main phase (20 UT, 9 Nov), which drives the CEJ in the nighttime equatorial ionosphere at YAP.

Fejer et al. (2007)

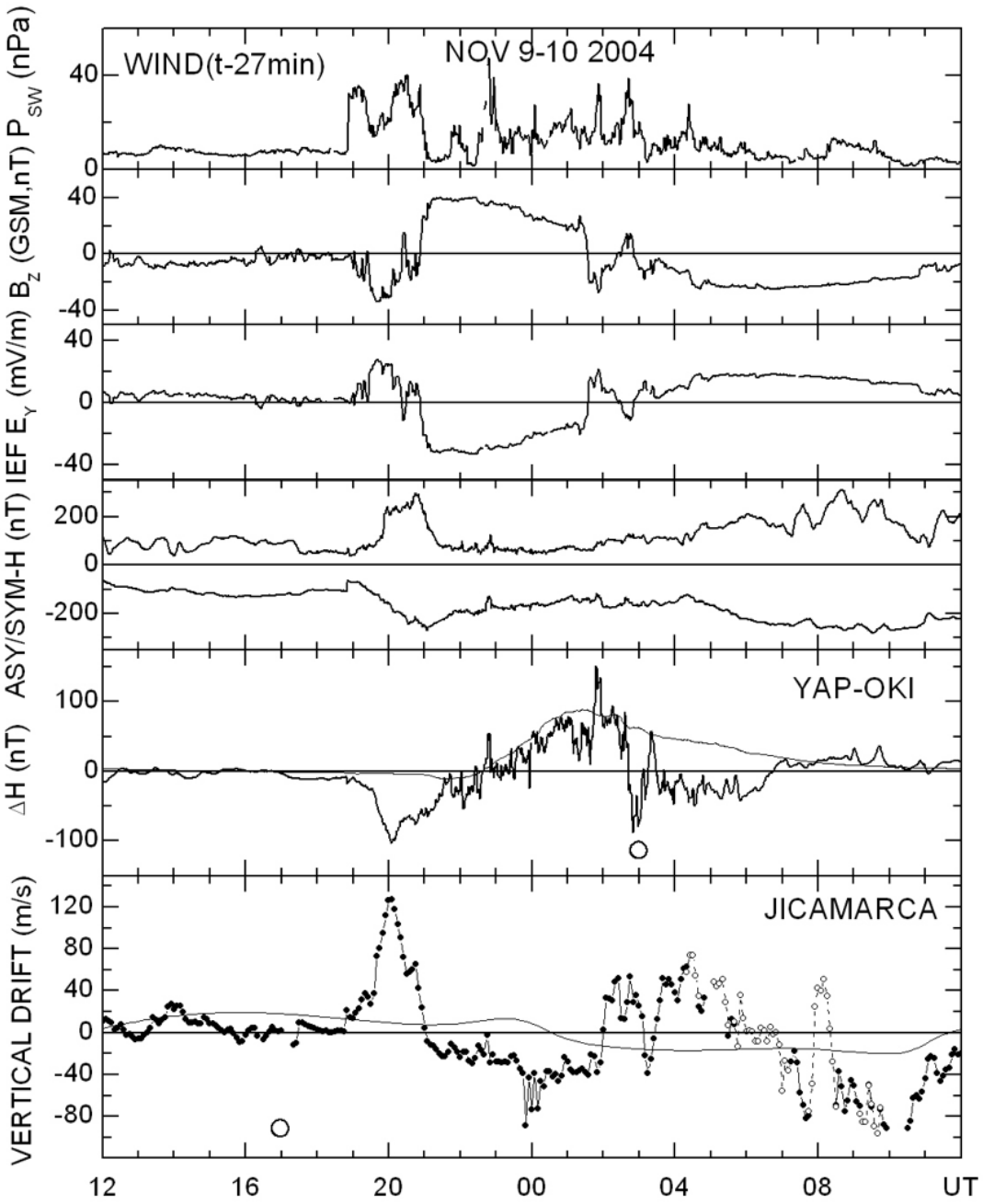

Near-instantaneous transmission of the SC electric field to low latitude

Preliminary impulse (PI) in high latitude

No PI at low latitude

Electric field of the PI at low latitude

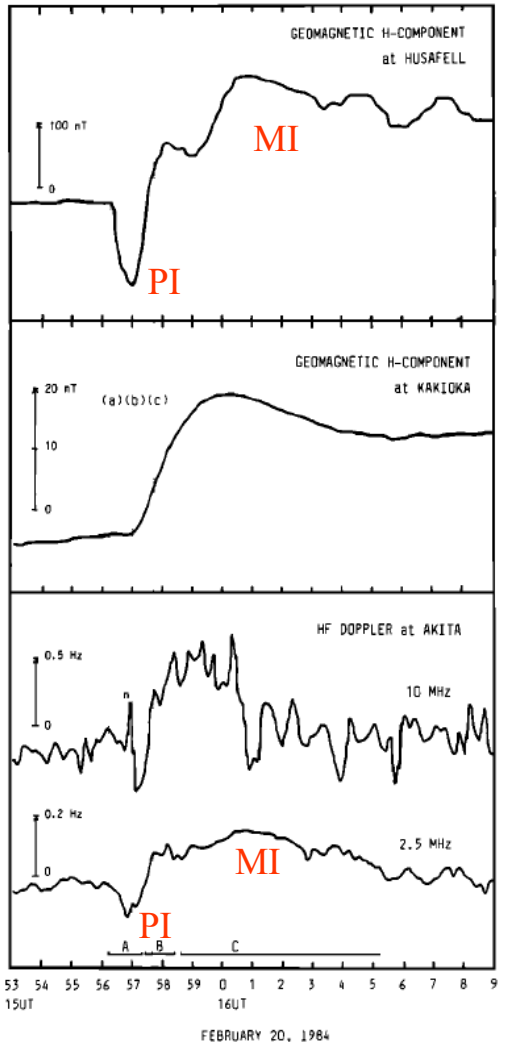

high latitude

Low latitude

(Kikuchi, JGR 1986)

Opposite polarity of the SC electric fields on the day- and night-sides with evening anomaly

HF Doppler frequency deviations caused by the SC electric fields of the type of (+-) in the day (top), (+-) in the evening (middle), and (-+) in the night (bottom), composed of the preliminary frequency deviation (1min) followed by the main frequency deviation (>5min). The eveningtime electric fields are in the same direction as those in the daytime.

Kikuchi et al. (2016)

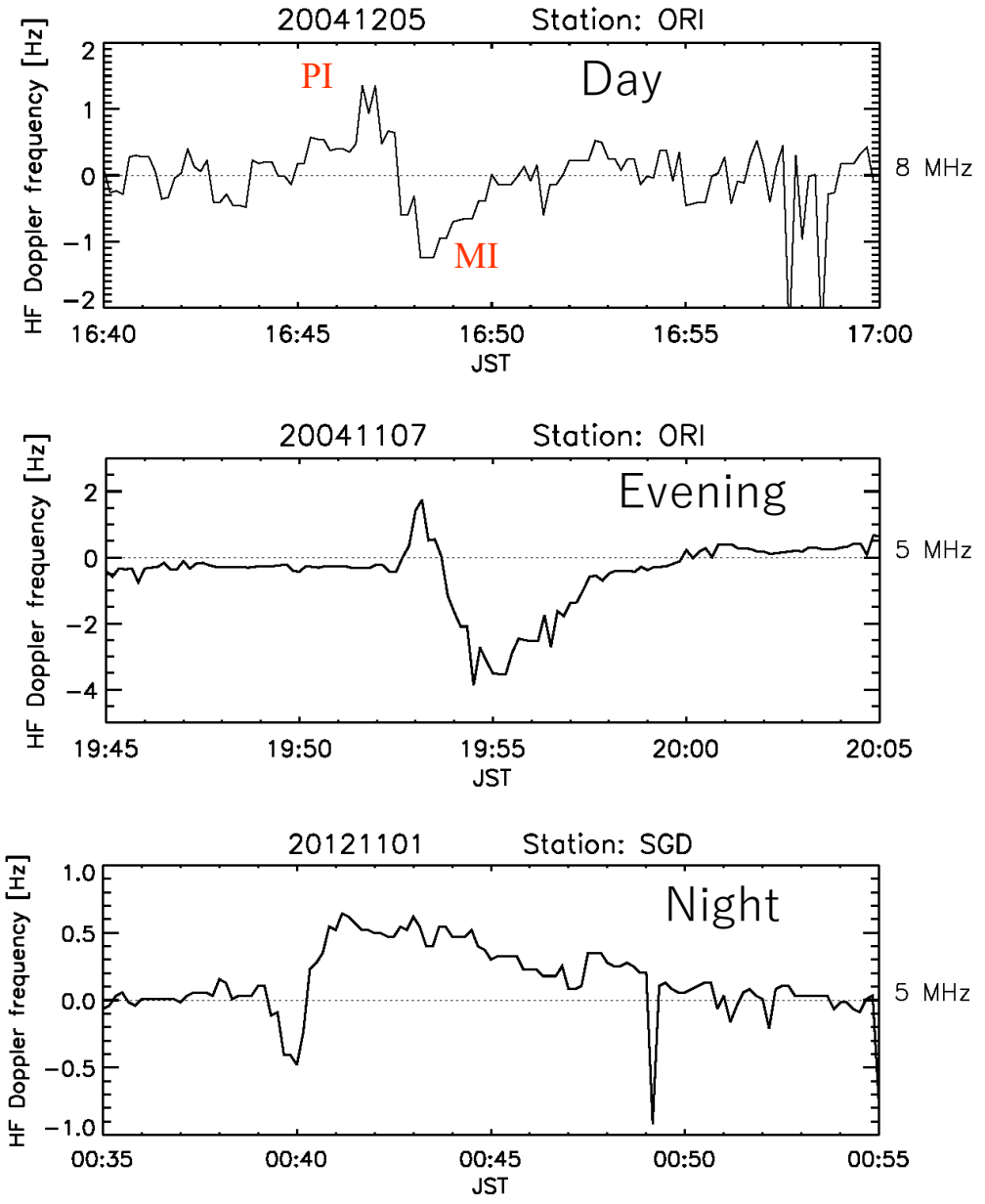

Reproduction of the SC electric fields by the Tanaka's global simulation

(Kikuchi et al., JGR 2016)

HF Doppler observation

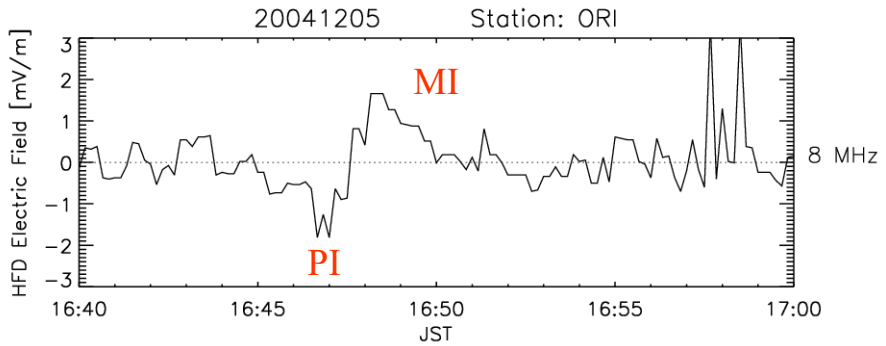

Day

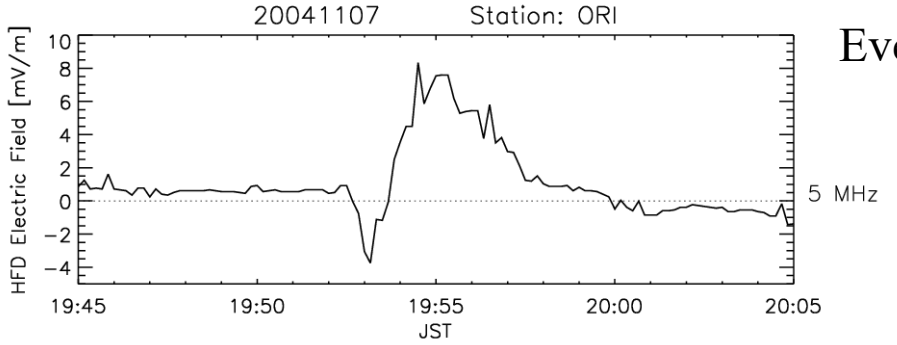

Evening

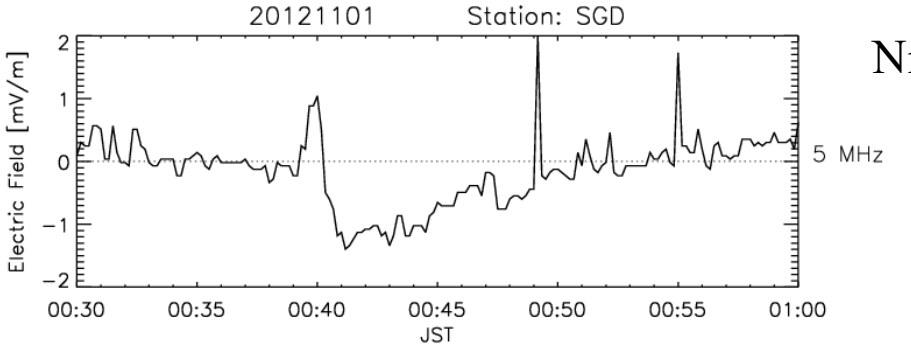

Night

Simulation

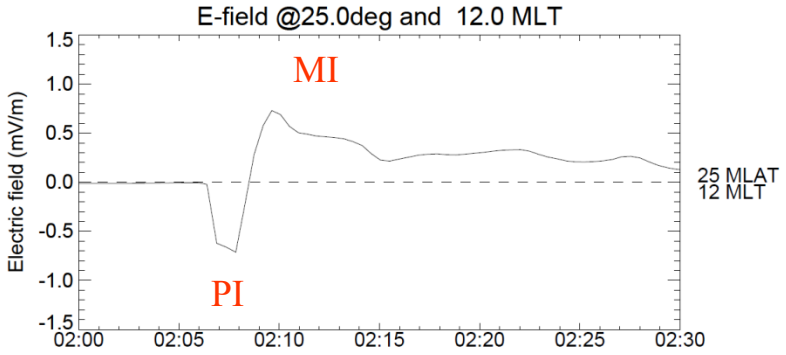

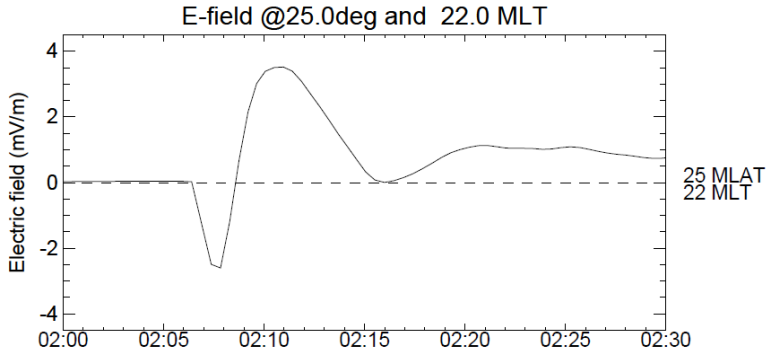

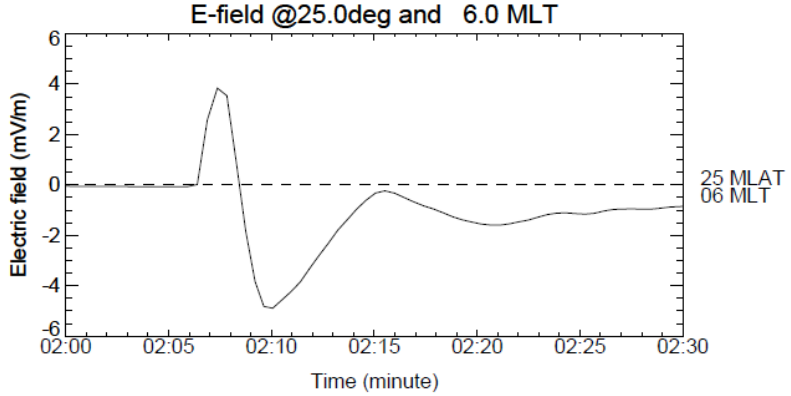

Electric fields with evening anomaly at high-equatorial latitudes (potential solver calculation)

Model calculations of eastward electric fields at 60° latitude (30° colatitude), 30° latitudes and the equator with the current continuity equation with an input of FACs. (picked out from the right panels of Figure 3a of Tsunomura (1999)). The electric field is calculated for four conductivity models with different Hall term, . The dot-dashed lines with number 1.0 are the most realistic model, showing outstanding evening anomalies of the ionospheric electric field at all latitudes.

Tsunomura (1999)

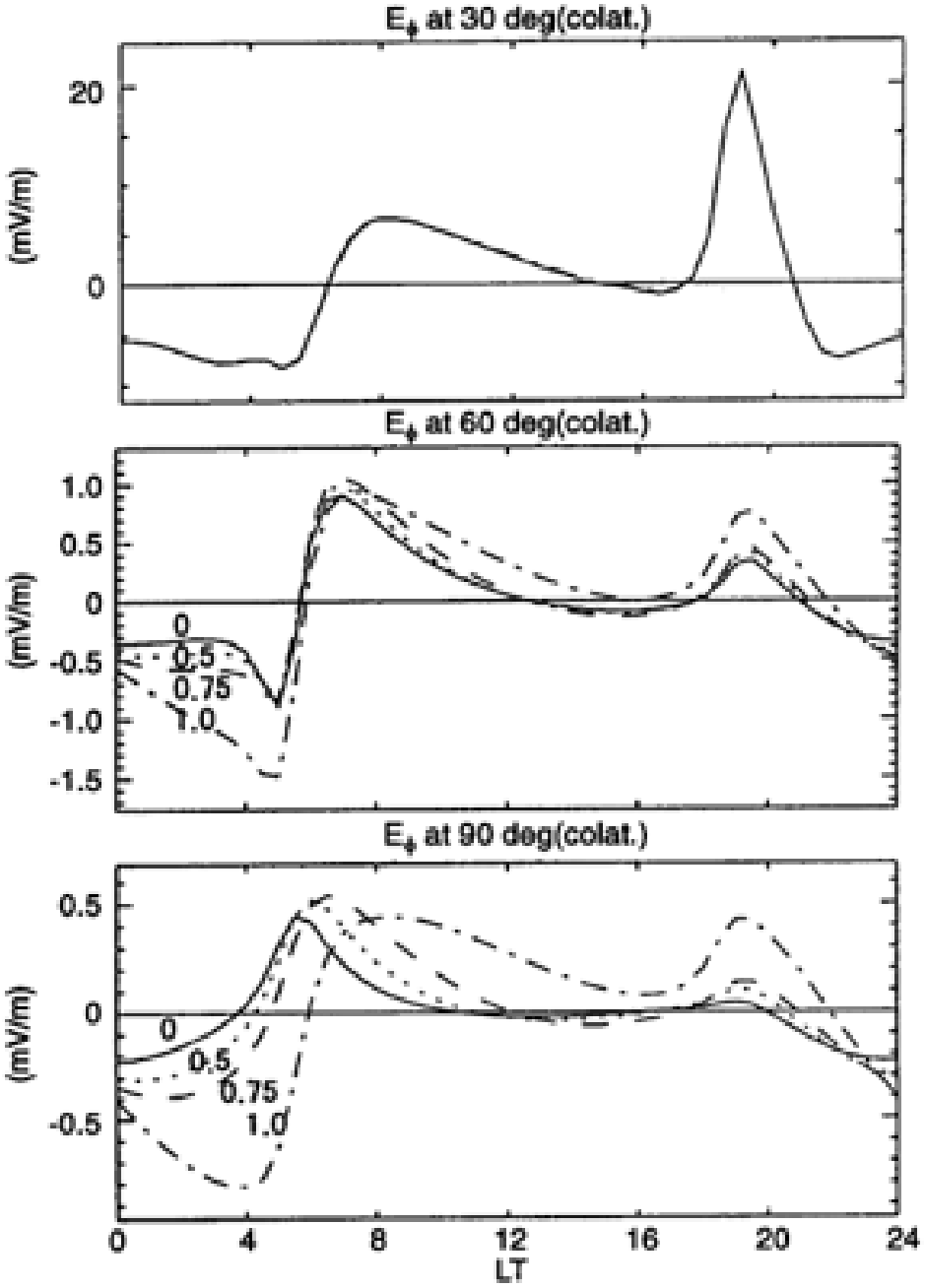

TM0 mode propagation of the ionospheric electric potential in the Earth-ionosphere waveguide

Three-layered Earth-ionosphere waveguide model explaining the instantaneous transmission of the electric potential ($+V_0$) and currents (J_{xI}) given by the downward field-aligned current (FAC(+)) at the left end of the model. The TM_0 mode wave consisting of the vertical electric field (E_{zV}) and horizontal magnetic field (H_{yV}) propagates at the speed of light, carrying electric currents in the ionosphere and on the ground and transporting the Poynting flux ($S_{xV} = E_{zV} \times H_{yV}$) to low latitude. A fraction of the Poynting flux ($S_{zI} = S_{xV}[x+\Delta x] - S_{xV}[x]$) is transmitted into the ionosphere, causing attenuation of the TM0 mode wave. The Poynting flux leaking to the magnetosphere (S_{zM}) drives plasma motion of F-region ionosphere.

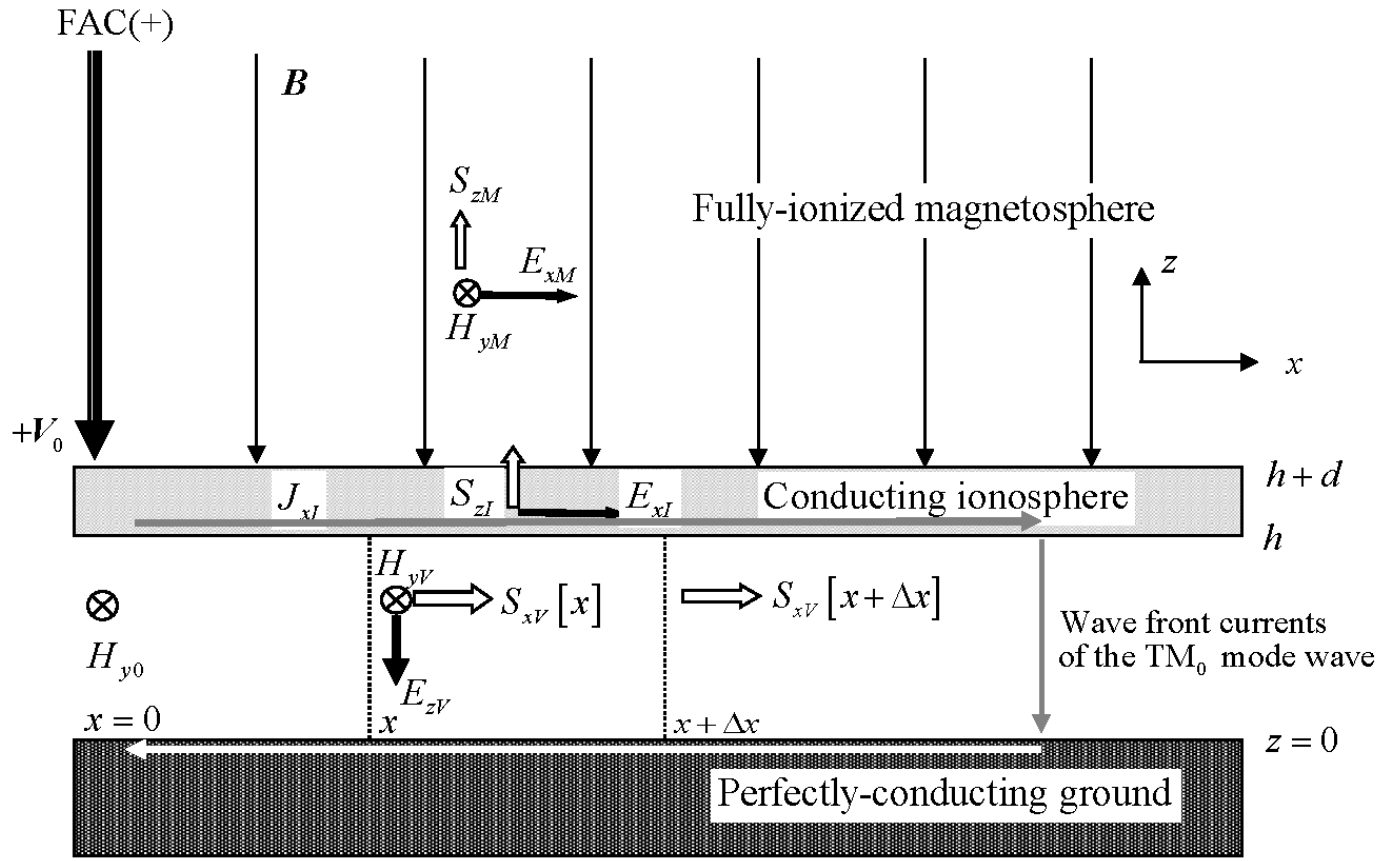

Kikuchi (2014)

Transmission of the magnetospheric electric potential and currents to the middle – equatorial latitudes through the polar ionosphere (Magnetosphere-Ionosphere-Ground transmission line model)

Magnetosphere-ionosphere-ground current circuit achieved by the transverse waves in the magnetosphere and by the TM_0 mode wave in the Earth-ionosphere waveguide. The east-west symmetry leads to the zero-potential in the noon-midnight meridian which can be replaced with the perfectly conducting sheets (dashed lines). Downward and upward currents of the same amount are supposed to connect the ionospheric currents to the ground surface currents in the duskside and dawnside current circuits driven by the positive and negative potentials, respectively. (Figure 12

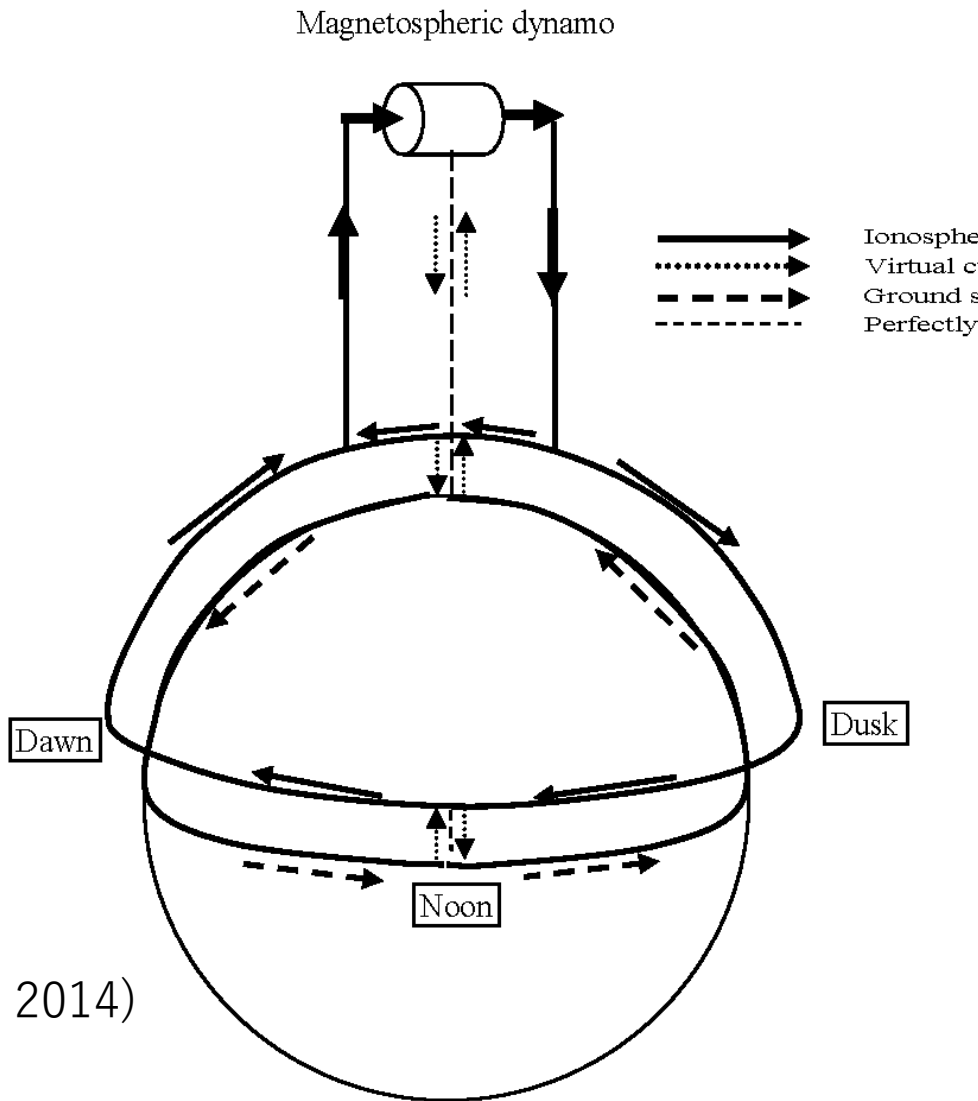

Kikuchi (JGR 2014)

Electric potential and currents at the (a) dynamo, (b) middle magnetosphere and (c) ionosphere in the magnetosphere-ionosphere transmission line

Electric potential, current, and power calculated at the (a) dynamo in the outer magnetosphere ( ), (b) mid-magnetosphere ( ), and (c) polar ionosphere ( ) of the MI transmission line (= 80,000 km) for the daytime ionospheric conductance (8 mho). The electric potential and internal resistivity of the dynamo are assumed to be 50 kV and 0 ohm, respectively, and the Alfven speed is 1000 km/s. The ionospheric electric potential and currents grow with the time constant of 13 min.

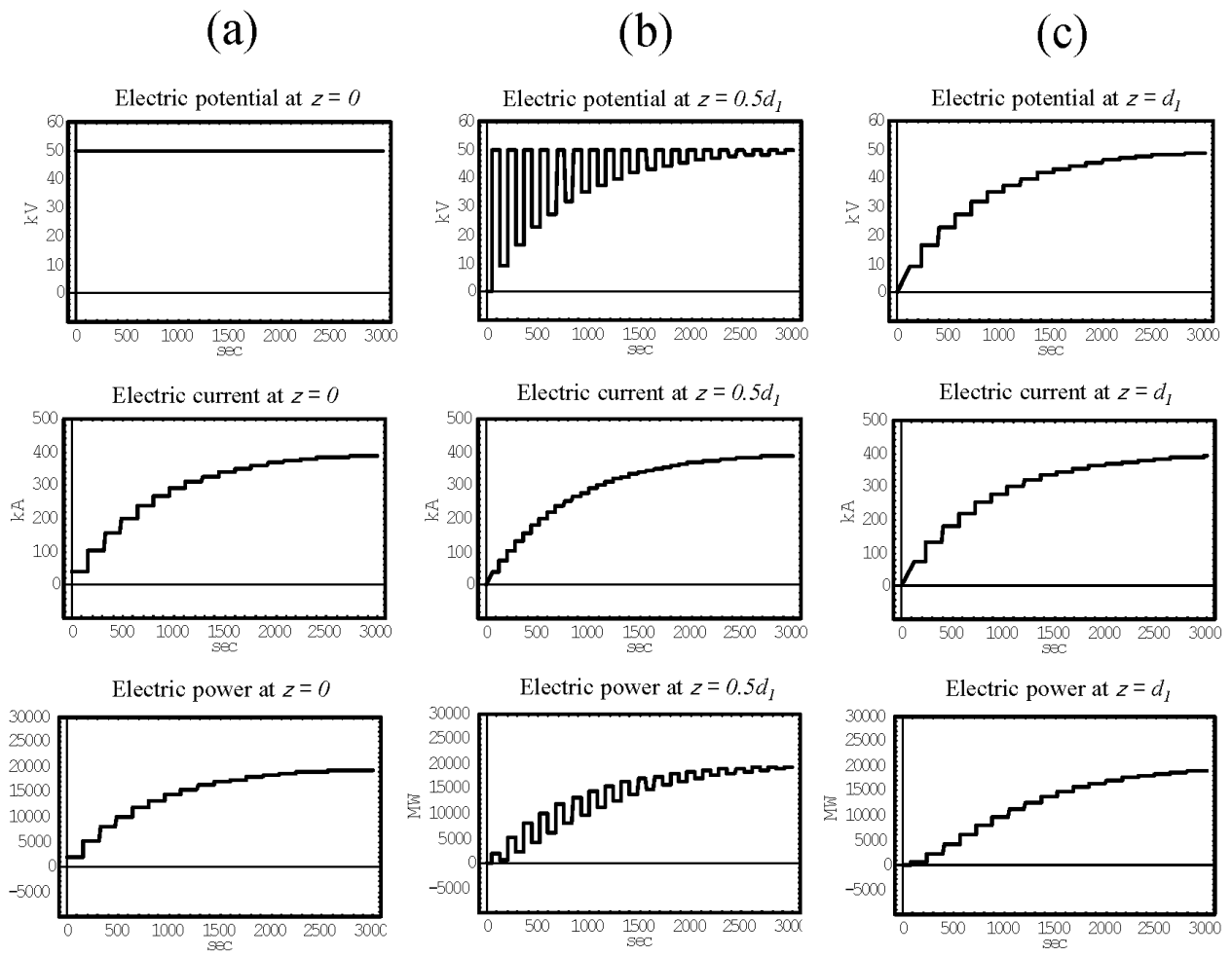

$$V_1(z,t) = V_0 \frac{Z_1}{r+Z_1}\left[\sum_{n=1}^{\infty}(\Gamma\Gamma')^{n-1}U\left(t-\frac{2(n-1)d_1+z}{V_A}\right)+\Gamma\sum_{n=1}^{\infty}(\Gamma\Gamma')^{n-1}U\left(t-\frac{2nd_1-z}{V_A}\right)\right]$$

Kikuchi (JGR 2014)

$$I_1(z,t) = V_0 \frac{1}{r+Z_1}\left[\sum_{n=1}^{\infty}(\Gamma\Gamma')^{n-1}U\left(t-\frac{2(n-1)d_1+z}{V_A}\right)-\Gamma\sum_{n=1}^{\infty}(\Gamma\Gamma')^{n-1}U\left(t-\frac{2nd_1-z}{V_A}\right)\right]$$

$$\Gamma=\frac{R_L-Z_1}{R_L+Z_1},\quad \Gamma'=\frac{r-Z_1}{r+Z_1}$$

Ionospheric currents in the Ionosphere-Ground transmission line as a function of the conductivity

(top two rows) The electric currents at x = 5000 km in the finite-length IG transmission line with the conductance of 100, 30, 10, 3, 1, and 0.3 mho, and (b) currents in the lumped-element circuit with 100, 10, and 1 mho. The time constant is 1-20s depending on the ionospheric conductance, longer for larger conductance. The lumped-element circuit well reproduces the current in the IG transmission line.

Kikuchi (JGR 2014)

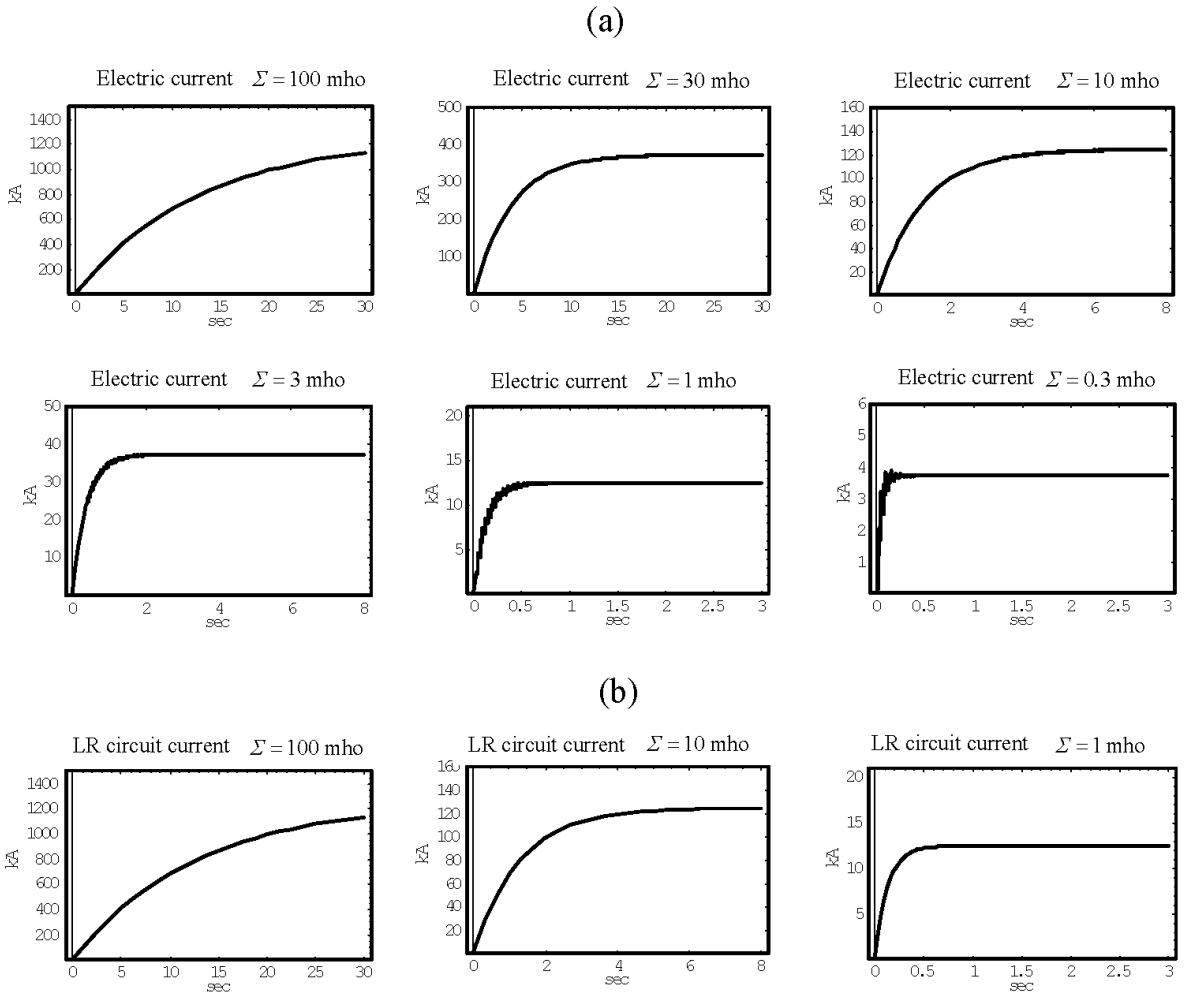

$$V(x,t) = V_0 \left\{ \sum_{n=1}^{\infty} \left[e^{-\frac{\alpha}{2} t_{n1}} U(t-t_{n1}) + \frac{\alpha}{2} t_{n1} \int_{t_{n1}}^{t} e^{-\frac{\alpha}{2}\tau} U(t-\tau) \frac{I_1\left(\frac{\alpha}{2}\sqrt{\tau^2 - t_{n1}^2}\right)}{\sqrt{\tau^2 - t_{n1}^2}} d\tau \right] - \sum_{n=1}^{\infty} \left[e^{-\frac{\alpha}{2} t_{n2}} U(t-t_{n2}) + \frac{\alpha}{2} t_{n2} \int_{t_{n2}}^{t} e^{-\frac{\alpha}{2}\tau} U(t-\tau) \frac{I_1\left(\frac{\alpha}{2}\sqrt{\tau^2 - t_{n2}^2}\right)}{\sqrt{\tau^2 - t_{n2}^2}} d\tau \right] \right\}$$

$$I(x,t) = V_0 \frac{1}{Z} e^{-\frac{\alpha}{2} t} \left\{ \sum_{n=1}^{\infty} U(t-t_{n1}) I_0\left(\frac{\alpha}{2}\sqrt{t^2 - t_{n1}^2}\right) + \sum_{n=1}^{\infty} U(t-t_{n2}) I_0\left(\frac{\alpha}{2}\sqrt{t^2 - t_{n2}^2}\right) \right\}$$

$$t_{n1} = \frac{2(n-1)d_2 + x}{c} \qquad t_{n2} = \frac{2nd_2 - x}{c} \qquad \alpha = \frac{R}{L} = \frac{1}{\mu_0 \Sigma \cdot h}$$

Summary

- **R1- and R2-FAC dynamos are created by the solar wind and magnetospheric plasma convection, respectively**.
- **DP2 fluctuations are caused by Hall currents at high latitude and Cowling currents at the equator, driven by the convection (R1 FACs) and overshielding (R2 FACs) electric fields**
- **R1 FAC-EEJ and R2 FAC-CEJ circuits are completed between the polar and equatorial ionosphere during the DP2 fluctuation events.**
- **Substorm CEJ and EEJ are caused by the R2 FACs (overshielding) on the day and nightside, respectively.**
- **Storm main phase EEJ and recovery phase CEJ are driven by the convection and overshielding electric fields.**
- **SC electric fields are potential fields with evening anomaly.**
- **Polar-equatorial current circuits are achieved near-instantaneously by TM_0 mode waves in the Earth-ionosphere waveguide.**
- **Magnetosphere-ionosphere-ground (MIG) transmission line model tells us that the FACs grow with time constant of the order of 10min, while the time constant of the ionospheric currents is 1-10s, which would result in different response of the ionosphere to the R1 and R2 FACs and alter their contribution on the ionospheric disturbances at low latitude.**